Quantum Chemical Analysis of Electronic Structure and n- and p-Type Charge Transport in Perfluoroarene-Modified Oligothiophene Semiconductors

Sharon E. Koh,[†] Bernard Delley,[‡] Julia E. Medvedeva,[§,||] Antonio Facchetti,[†] Arthur J. Freeman,[*,§] Tobin J. Marks,[*,†] and Mark A. Ratner[*,†]

Department of Chemistry and Materials Research Center, Northwestern University, Evanston, Illinois 60208, Paul Scherrer Institut, CH-5232 Villigen, PSI Switzerland, and Department of Physics and Astronomy and the Materials Research Center, Northwestern University, Evanston, Illinois 60208

Received: July 28, 2006

Density-functional theory (DFT) is employed to investigate the structural, electronic, and transport properties of several isomeric fluoroarene-oligothiophene-based semiconductors. Three oligothiophene systems varying in the perfluoroarene group positions within the molecule are studied to understand the electronic structure leading to the observed mobility values and to the n- or p-type behavior in these structures. Analyses of both intermolecular interactions in dimers and extended interactions in crystalline structures afford considerable insight into the electronic properties and carrier mobilities of these materials, as well as the polarity of the charge carriers. From the calculated carrier effective masses, we find that sterically governed molecular planarity plays a crucial role in the transport properties of these semiconductors. Our calculations correlate well with experimentally obtained geometries, highest-occupied molecular orbital (HOMO)/lowest-unoccupied molecular orbital (LUMO) energies, and the experimental carrier mobility trends among the systems investigated.

I. Introduction

Conducting soft materials are important for the development of organic-based electronics and optoelectronics.[1−3] However, many fundamental questions concerning how charge is transported through functional organic molecular solids are currently unresolved. For instance, why certain molecular materials have particular majority charge-carriers (electrons or holes) and how molecular and crystal structure parameters influence the relative magnitudes of carrier mobility are far from being completely understood.[2,4,5] For these materials to achieve full potential requires better understanding of both molecular properties and intermolecular interactions. It is well-known that the carrier mobility of organic conductors depends crucially on the geometry of molecular packing and that the carrier sign may be altered through introduction of substituents on the conjugated core.[6−8] In this regard, thiophene-based conductors are of great interest because of their attractive properties, including chemical/thermal stability, synthetic tailorability, solubility/processability, and relatively large carrier mobility.[9−15] The transport properties of the oligothiophene skeletons have been shown to be strikingly sensitive to the nature of the skeletal functionalization.[7,8,16] For instance, by the introduction of electron-withdrawing fluorocarbon substitutents, the energies of unoccupied orbitals can be lowered, making n-type transport channels available.[7,8,17−24] To date, most organic semiconductors have been found to be p-type charge transporters.[25−40] However, carriers of both signs are critically needed for organic CMOS (complementary metal oxide semiconductor) to increase operating speeds and to reduce power consumption.

In the quest for n-type organic conductors, recent research in this laboratory has focused on fluorocarbon-oligothiophene isomers containing variously positioned perfluorinated-arene and alkyl substituents.[14,15,17,41] Experimentally, we have used field-effect transistor (FET) measurements to observe substantial mobilities and n-type carrier dominance, a striking variance from the p-type transport typical of unfunctionalized and hydrocarbon-functionalized oligothiophenes.[7,8,17,28,42−45] This contribution provides theoretical investigations of perfluoroarene-modified oligothiophenes that are of interest because of their unusual semiconducting properties; in particular, relatively large carrier mobilities combined with favorable reduction properties resulting in n-type transport.[17,41] Here, we focus on the electronic and structural properties of three electrically and crystallographically characterized mixed-polarity molecules with perfluoroarene groups sequentially located in different skeletal positions; each molecule contains six rings, two perfluoroarene units, and four thiophene rings (see Figure 1). As Table 1 shows, both **TFTFT** and **FTF** exhibit large FET mobilities, with the latter exhibiting n-type transport. The archetypical p-type conductor **6T** is also investigated for comparison.[46] To understand the effect of the molecular structure on the electronic and transport properties (i.e., the majority carrier sign inversion and variation in the carrier mobility magnitudes) in the three perfluoroarene-modified thiophene semiconductors, the electronic and geometric structures were investigated using two density functional theory (DFT) methods. First, a molecular quantum chemical approach focused on understanding frontier orbital interactions and charge density distributions arising from pairwise intermolecular interactions, starting from the crystal packing of dimers and idealized $\pi-\pi$ stacked models. Second, we study electronic properties of the corresponding crystalline structures with an infinite three-dimensional network by calculating their electronic band structures, conduction/valence band topologies, and electron/hole effective masses. The latter

* To whom correspondence should be addressed.
[†] Department of Chemistry and Materials Research Center.
[‡] Paul Scherrer Institut.
[§] Department of Physics and Astronomy and the Materials Research Center.
[||] Current address: Department of Physics, University of Missouri−Rolla, Rolla, MO 65409.

10.1021/jp064840x CCC: $33.50
Published on Web 11/11/2006

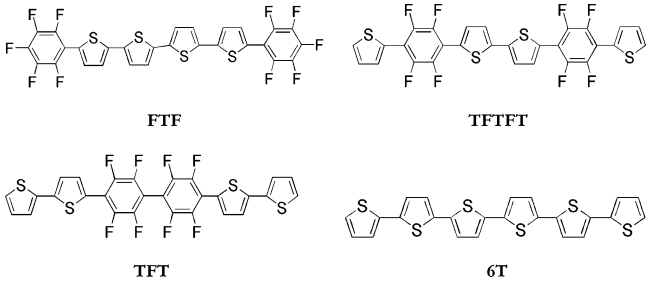

Figure 1. Molecular structures examined in this study.

approach contrasts with most of the band structure studies of organic conductors performed to date which have predominantly been limited to one-dimensional analyses in reciprocal space (because of the inherent structural complexity of most molecular crystals).[47−51]

The band structure calculations reported here suggest, for each of the three perfluoroarene-modified oligothiophene semiconductors, similar transport properties for both hole and electron carriers. It will be shown that molecular geometry and packing dictate the $\pi-\pi$ overlap connected with the crystallographic direction of the highest transport observed in most organic conductors, as well as in the present calculations. Importantly, our calculations agree well with experimentally obtained crystal structure geometries, electrochemically measured redox potentials, and the observed mobility trends.

II. Computational Methods

Density functional theory (DFT) has been found to be an accurate formalism for calculating the chemical and structural properties of many molecular systems, including organic conductors.[52−58] The DFT methodology has also been shown to predict accurate band structure diagrams, bandwidths, and densities of states for conventional inorganic semiconductors and to provide reliable trends for organic conductors.[59−61] Despite the well-known overbinding effects of pure DFT functionals which result in underestimations of the energy band gaps, full band structure analyses can provide information on the band topology for the top of the valence band and the bottom of the conduction band and thus illuminate features such as carrier effective masses, carrier mobilities, and transport symmetries that are difficult to extract from simple dimer models. The two methods used in this study are detailed below.

A. Molecular Approach. Monomer and dimer calculations were performed with DFT using the Q-Chem 2.1 program[62] with the B3LYP hybrid functional[63,64] and a 6-31G* basis set. Optimized monomer geometries were compared to those obtained experimentally via X-ray diffraction.[17] Three dimer models were investigated: the true dimer, a modified dimer, and the perfect dimer models (see Figure 2). In the true dimer model, the atomic geometry is extracted directly from the crystallographically determined unit cell. In the **FTF** and **TFT** systems, the true dimer is significantly slipped from a cofacial arrangement, with two neighbor half-molecules overlapping. Therefore, a modified dimer was investigated for **FTF** and **TFT** where two-half-molecules interact with one full molecule. In the perfect dimer, optimized monomers are used to construct the dimer with two monomers spaced at the crystallographically determined cofacial distance (see Figure 3a for cofacial packing). This distance is 3.2 Å for **FTF**, 3.4 Å for **TFTFT**, and 3.36 Å for **TFT**.

Single-point energy calculations were performed for all dimer structures, retaining the crystal geometry in the two models referred to here as the true dimer and the modified dimer and freezing the cofacial spacing in the third model, the perfect dimer. DFT calculations were performed in Q-Chem 2.1 and Jaguar 5.0.[65] Orbital plots were calculated using single-point energy calculations with Spartan '04 for Windows,[62,66] using DFT with a B3LYP functional[63,64] and 6-31G* basis set.

B. Band Structure Calculations. Electronic structure calculations were performed with DMol^3 3.8[53,67] using DFT with the Perdew-Wang exchange-correlation functional[68,69] and a DND basis set.[67] The lattice parameters and the atomic positions were taken from experimentally determined crystal structures (see Figure 3b for crystallographic packing).[17] For sexithiophene (**6T**), the structural parameters were taken from the Cambridge Crystal Database.[70,71] For all systems under investigation, the internal geometries were optimized by total energy and atomic force minimization; during the relaxation, the volume of the corresponding unit cell was fixed to the experimental value. The results showed that the binding energies changed ∼1%, while, as expected, the band gap values became smaller upon optimization, ranging from 0.09 to 0.21 eV.

The electronic band structures were calculated along the high-symmetry directions in the corresponding standard Brillouin zone of the designated crystal system. For better comparison among the systems and because of the peculiar space orientation of the molecules, additional band structure calculations were performed including other directions in reciprocal space. Densities of states were calculated using the tetrahedron method[72] and a 8 × 8 × 4 k-point mesh (see Figure 1 for molecular structures for **FTF**, **TFTFT, TFT,** and **6T**). Finally, both the hole and electron effective masses were calculated according to

$$\left[\frac{1}{m^*(k)}\right]_{i,j} = \pm\frac{1}{\hbar^2}\frac{\partial^2 E}{\partial k_i \partial k_j} \qquad (1)$$

Here, m^* is the effective mass, E is the band energy, and k is the wavevector. Note that the estimation of curvature can be dependent on different numerical methods for estimating the second derivative of energy with respect to k-space. Here we use a variation of the three-point method commonly used for estimating second derivatives.

III. Results

In the discussion below, differences in structural and electronic properties are compared for **FTF**, **TFTFT**, and **TFT** in both optimized gas phases and crystalline structures. Dimer interactions are evaluated using three different models to understand intermolecular interactions. Additionally, band structure calculations are used to understand the extended polycrystalline networks of these organic semiconductors. From these calculations, the electronic structure properties defining charge transport are then evaluated.

A. Energetics and Structural Properties of Monomers. DFT-optimized gas-phase structures generally correspond well with the experimental crystallographic data. For the systems herein, we find that DFT overestimates the C−S bond lengths within the thiophene ring (0.02 Å) and the conjugated C−C bonds lengths within the thiophene ring (0.01 Å), while the C−C single bond lengths between rings are underestimated by <0.008 Å. In comparison to the computed geometry, the experimental dihedral angles in **FTF** are smaller between the two *cis*-thiophene rings by 5.5° but are slightly larger between the perfluoroarene groups and the two sets of *cis*-thiophene groups (by 1.5°). For **TFTFT**, the dihedral angles are all slightly (1−7°) greater in the experimental crystal geometry. For **TFT**, the

TABLE 1: Experimental Electrochemical Data (eV), Where Electron Affinity (EA) and Ionization Potentials (IP) Are Estimated via Redox Potentials Measured versus SCE,[17,41] Experimental Mobilities (measured in field-effect transistors), Where the Temperature Reported is the Deposition Temperature (T_D) of the Organic Film, and Computed Band Gaps (eV)[a]

	experimental electrochemistry data[17] (eV)						calculated band gaps (eV)		measured[17,41] μ_{FET} ($cm^2V^{-1}s^{-1}$)
	EA THF	IP THF	E_{gap} THF	EA film	IP film	E_{gap} film	E_{gap} band structure	E_{gap} molecular	FET μ (T_D in °C)
FTF	−2.85	−5.48	2.63	−2.69	−5.27	2.58	1.44	2.80	0.08 (60)[b] 0.43 (90)[b]
TFTFT	−2.82	−5.64	2.82	−2.67	−5.32	2.65	1.72	2.91	0.01 (60)[c] 0.004 (90)[c]
TFT	−2.81	−5.81	3.00	−2.53	−5.40	2.87	1.97	3.18	4×10^{-5} (60)[c] not active (90)
6T	−2.65	−5.20	2.55	−2.36	−4.78	2.42	1.38	2.61	0.03 (60)[c]

[a] Note that the gaps calculated for the band structure were with a pure DFT (LDA) functional and the molecular calculations were with a hybrid functional. [b] n-type conductor. [c] p-type conductor.

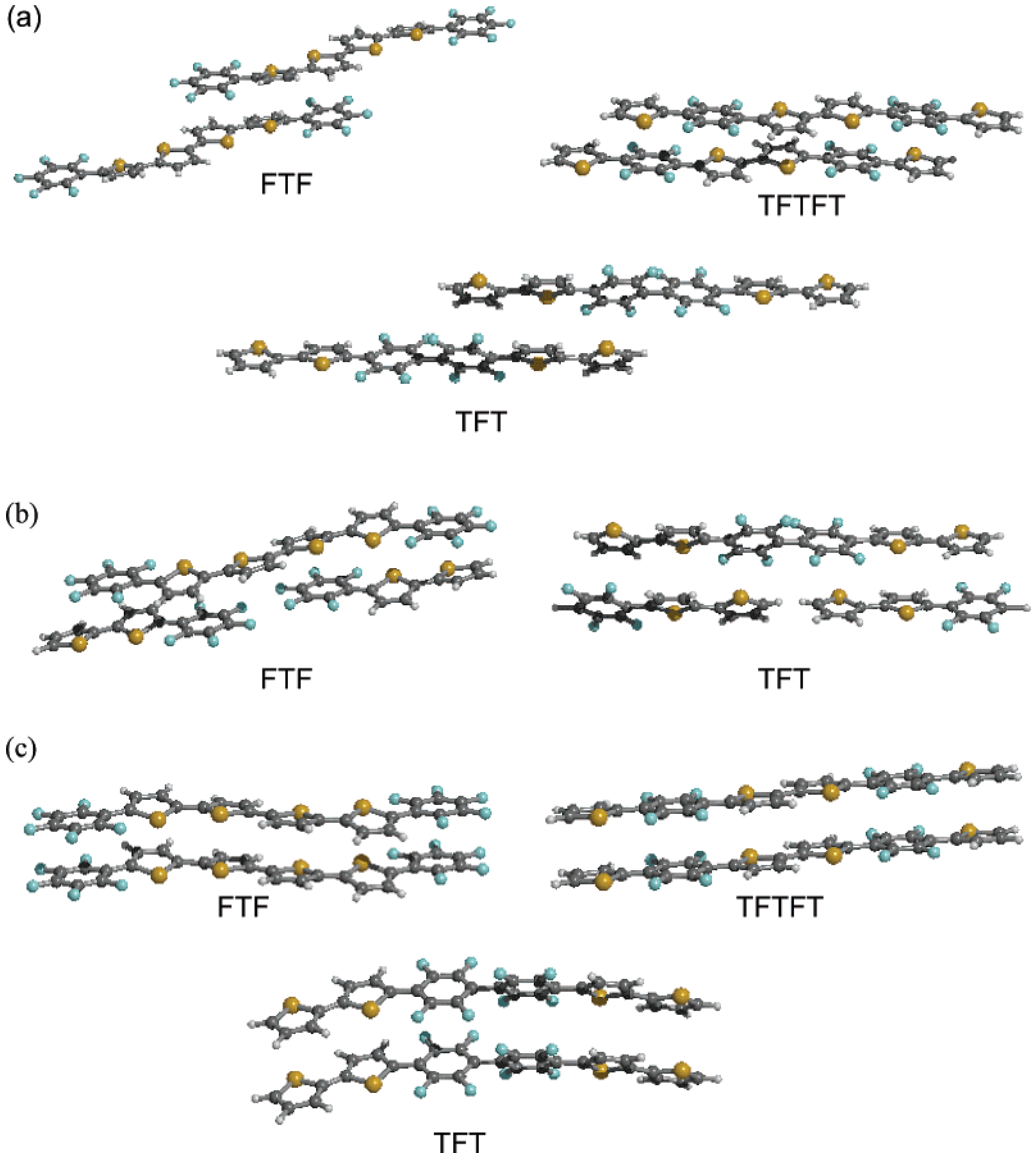

Figure 2. Schematics of (a) the true dimers from the crystal, (b) the modified dimers from the crystal, and (c) the perfect $\pi-\pi$ overlap dimers.

dihedral angle between the two perfluoroarene groups is measured to be 53.9(0.32)° in the crystal structure[17] versus 52.6° in the optimized structures. All other dihedral angles in the crystal geometry are greater (by 2−7°) than in the optimized single-molecule structure of **TFT**.

Orbital contour plots for the three molecules in both optimized gas-phase and crystal geometries reveal that both highest-occupied molecular orbitals (HOMOs) and lowest-unoccupied molecular orbitals (LUMOs) consist of linear combinations of individual thiophene and perfluoroarene groups. The HOMOs reside predominately in the thiophene rings and show the typical *cis*-butadiene HOMO pattern (Figure 4); there is some, minimal, contribution from the perfluorarene segments. The LUMOs, on the other hand, are more delocalized with more equal contribution from both the thiophene and perfluoroarene groups. Substantial contributions from the sulfur atoms are also seen in

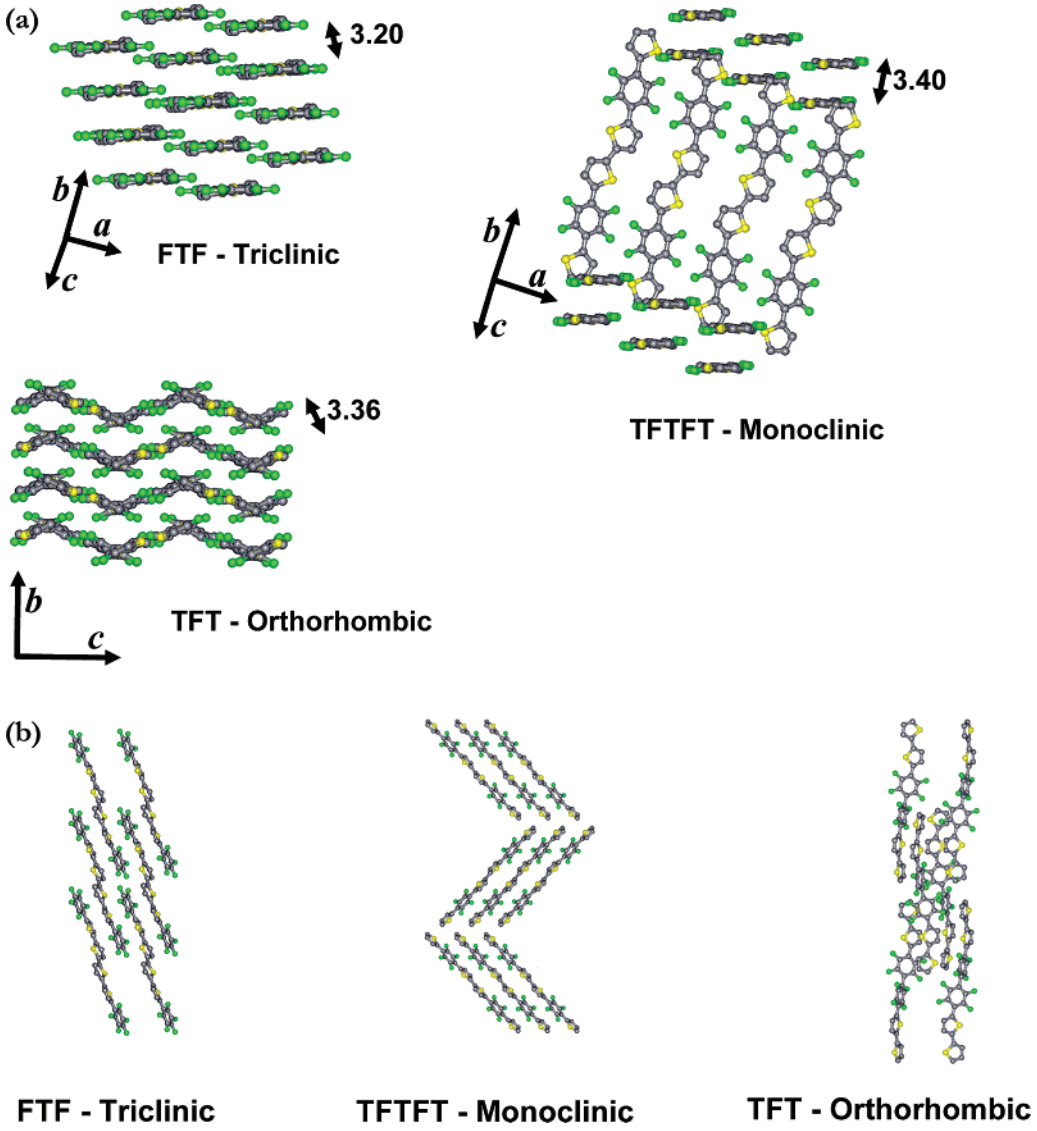

Figure 3. Experimental crystal packing diagrams[17] for the molecules examined in this study: projections showing the (a) cofacial packing and (b) molecular packing.

the LUMO orbital plots, whereas the fluorine atoms make little direct contribution to either HOMO or LUMO orbitals (in keeping with the traditional role of fluorine as an inductive substituent). Additionally, the carbon-centered orbitals of the perfluoroarene fragments in **TFTFT** and **TFT** show significantly more charge density localization than **FTF**. HOMO/LUMO energies from the crystal geometries exhibit slightly larger energy gaps than in the optimized gas-phase structures by 0.082 eV for **FTF**, 0.109 eV for **TFTFT**, and 0.190 eV for **TFT**.

Molecular orbital contour plots for the dimers [denoted as $(\mathbf{FTF})_2$, $(\mathbf{TFTFT})_2$, and $(\mathbf{TFT})_2$] in the enforced perfect $\pi-\pi$ overlap model reveal significant intermolecular orbital overlap between the LUMO oribitals in both $(\mathbf{FTF})_2$ and $(\mathbf{TFTFT})_2$. This is especially significant between corresponding C···C and the S···S pairs in the two cofacial molecules, which exhibit intermolecular contacts of 3.2 and 3.4 Å, respectively. In $(\mathbf{TFT})_2$, orbital overlap is far smaller than in $(\mathbf{FTF})_2$ and $(\mathbf{TFTFT})_2$ because of the pronounced twist from planarity in the molecular geometry, which leads to a far larger interplanar spacing. See Figure 5 for example of contour plot of the $(\mathbf{FTF})_2$ dimer in the perfect model.

B. Bandwiths in Dimers: Tight-Binding Model. In a simple tight-binding model picture, bandwidths arising from orbital splittings directly determine the mobility (increased bandwidth leads to increased mobility). This bandwidth follows from the tight-binding model picture where the monomer HOMO and LUMO orbitals split upon formation of an interacting dimer (see Figure 6).[73] Orbital splittings are defined by the absolute energy difference between the HOMO and HOMO−1 ($2\beta_{\mathrm{HOMO}}$) and the LUMO and LUMO+1 ($2\beta_{\mathrm{LUMO}}$) orbital energies (see Figure 2). Computed bandwidths are 4β[74] and are summarized in Table 2.

1. True Dimers. Dimers with the atomic positions taken directly from the corresponding crystal geometry were also evaluated (Figure 2a). In $(\mathbf{TFTFT})_2$, there is little slippage in the packing, with a slight displacement in the parallel planes between the two molecules in the dimer. The bandwidths obtained for $(\mathbf{TFTFT})_2$ are 0.164 (HOMO) and 0.272 eV (LUMO). In both $(\mathbf{FTF})_2$ and $(\mathbf{TFT})_2$, the monomer cofacility is slipped, reducing the interaction. For $(\mathbf{FTF})_2$, bandwidths of 0.284 (HOMO) and 0.112 eV (LUMO) are computed, while $(\mathbf{TFT})_2$ has bandwidths of 0.224 (HOMO) and 0.096 eV (LUMO) (Table 2). In **6T**, the herringbone pattern of the molecular structures are perpendicular, leading to reduction in perfect $\pi-\pi$ overlap. The bandwidths obtained for $(\mathbf{6T})_2$ are 0.276 (HOMO) and 0.271 eV (LUMO).

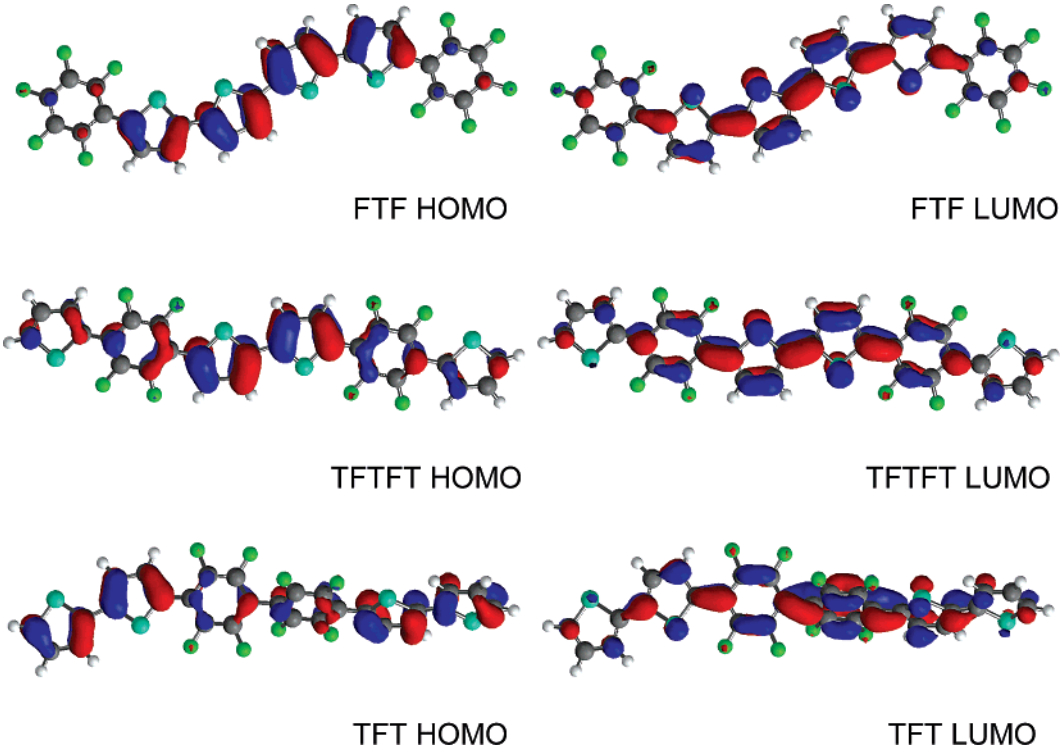

Figure 4. Monomer molecular orbital contour plots of the HOMO and LUMO orbitals of **FTF**, **TFTFT**, and **TFT**.

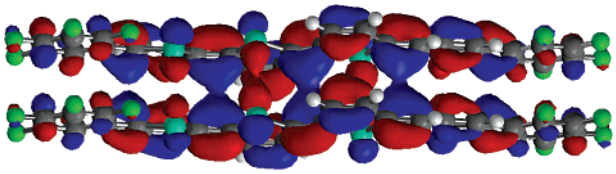

Figure 5. Example orbital plot. A contour plot of **(FTF)$_2$** in the perfect dimer model. The molecular orbital contour plot reveals the overlap in charge density.

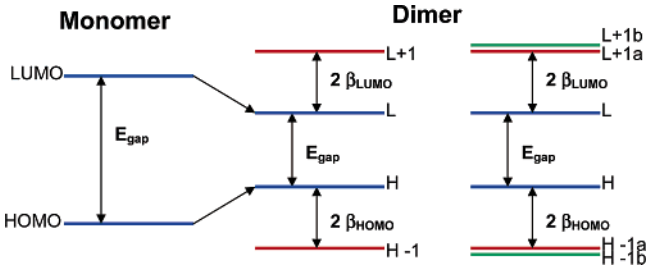

Figure 6. Energy splittings used to determine bandwidths. Cartoon of a monomer evolving into a dimer band diagram. The left most dimer model corresponds to the band diagram for the dimers in the perfect and true dimer models. The dimer band diagram on the right corresponds to the modified dimer model. Here, orbital splitting corresponds to 2β and E_{gap} to the HOMO/LUMO energy gap (H═HOMO, L═LUMO). Note that in this model the bandwidth is 4β.[74]

2. Modified Dimers. The interactions within **(FTF)$_2$** and **(TFT)$_2$** were further investigated with a modified dimer model, using two half molecules interacting with a full molecule in the corresponding crystal lattice packing (Figure 2b). The scission points of the half molecules were capped with hydrogen atoms.

A comparison of the energy splitting patterns traced from the monomers to the modified dimers reveals that the presence of the two half molecules results in the appearance of additional orbitals having energies both lying within 0.001 hartree (0.027 eV), Figure 2 (designated as HOMO−1a and HOMO−1b for the HOMO levels and similarly LUMO+1a and LUMO+1b for the LUMO). Here, the HOMO−1a and LUMO+1a have orbital energy values close to the HOMO and LUMO orbitals. Bandwidths were calculated from the HOMO/HOMO−1a and LUMO/LUMO+1a energy differences. As expected, the bandwidths of the modified dimers are increased by 1−3 and 6−8 times for the HOMO and LUMO, respectively, as compared to the true dimers, see Table 2, showing the significance of the interactions: **(FTF)$_2$** is found to have bandwidths of 0.878 (HOMO) and 0.852 eV (LUMO), and **(TFT)$_2$** has bandwidths of 0.262 (HOMO) and 0.612 eV (LUMO) (Table 2).

3. Perfect Dimers. To understand the perfect $\pi-\pi$ stacked system for the three molecules under investigation, orbital energy calculations on fully eclipsed dimers with incrementally varied *z*-axis spacings (distances between the cofacial molecular $\pi-\pi$ stacking) were also performed (Figure 2c). Bandwidths were found to decrease exponentially with respect to the distance between the two molecules. As *z* becomes greater than 5 Å, the two molecules in the dimer behave essentially like two isolated monomers with orbital energies corresponding to those of the monomer.

Bandwidths (4β) reported from this model are for crystallographically determined $\pi-\pi$ cofacial distances [**(FTF)$_2$** 3.2 Å, **(TFTFT)$_2$** 3.4 Å, and **(TFT)$_2$** 3.36 Å]. Bandwidths are estimated to be 1.688 (HOMO) and 1.198 eV (LUMO) for **(FTF)$_2$** and 1.414 (HOMO) and 1.306 eV (LUMO) for **(TFTFT)$_2$**. In **(TFT)$_2$**, the large dihedral angle between the two perfluoroarene groups leads to small bandwidths: 0.544 (HOMO) and 0.380 eV (LUMO). The corresponding bandwidths for **(6T)$_2$** are found to be 1.258 (HOMO) and 1.244 eV (LUMO). Bandwidths obtained via this orbital splitting analysis are summarized in Table 2.

C. Band Structures of the Crystals. Band structures were investigated by evaluating band dispersion along standard Brillouin zones and additional directions in the reciprocal space for all four systems: **FTF** (triclinic), **TFTFT** (monoclinic), **TFT** (orthorhombic), and **6T** (monoclinic). Using the standard Brillouin zone directions, we found less dispersion than with

TABLE 2: Summary of HOMO and LUMO Splittings from Molecular Orbital Calculations at the B3LYP/6-31G* Level of Theory[a]

	true dimer from crystal (a)		modified dimer from crystal (b)		perfect $\pi-\pi$ overlap dimer (c)	
	HOMO (eV)	LUMO (eV)	HOMO (eV)	LUMO (eV)	HOMO (eV)	LUMO (eV)
FTF	0.284	0.112	0.878	0.852	1.688	1.198
TFTFT	0.164	0.272	NA	NA	1.414	1.306
TFT	0.224	0.096	0.262	0.612	0.544	0.380
6T	0.276	0.271	NA	NA	1.258	1.244

[a] See Figure 2a−c for dimer configurations chosen for the molecular systems. The cofacial spacing for the perfect dimer model is as follows: **FTF** (3.2 Å), **TFTFT** (3.4 Å), and **TFT** (3.36 Å)

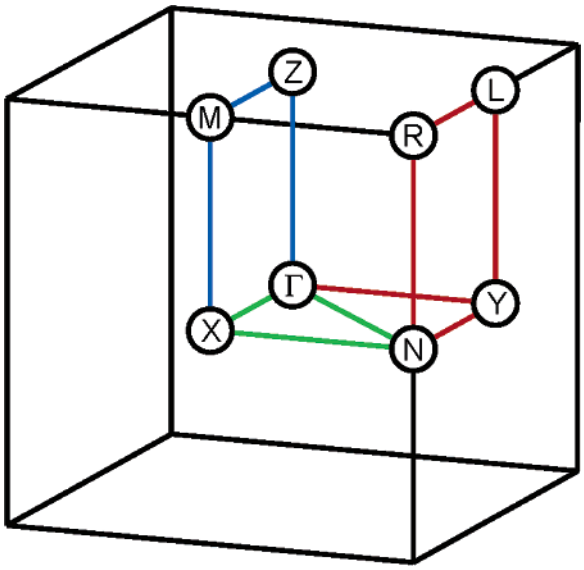

Figure 7. Schematic of the additional points evaluated in reciprocal space used to generate the band structure plots seen in Figure 8.

the inclusion of additional directions in reciprocal space in the band structure plots, where larger energy dispersion of both the conduction and valence bands is found for all structures investigated, but it most pronounced in the **FTF** system. This additional band dispersion is the result of a more thorough sampling in the reciprocal space of the molecular packing (Figure 7). Thus, we may conclude that more directions, as compared to the standard directions in the Brillouin zone, are required to obtain accurate band dispersions and, therefore, to describe more accurately the charge-transport properties through analysis of the effective masses at the conduction and valence band edges. Herein, we discuss the findings in band structure plots taken from the additional reciprocal space evaluation as seen in Figure 8; the results are summarized in Table 3.

The effective mass values calculated at the conduction band edge (CBE) and valence band edge (VBE) predict the following mobility trends: **FTF** > **TFT** > **TFTFT** > **6T**. It is expected that the geometric twist in **TFT** should lead to a much lower charge transport; however, this is not seen in the comparison of effective mass calculation at the CBE and VBE. Overall band dispersion, as monitored by the bandwidths seen in the band structure plots (Figure 8), is smaller in **TFT** than in the other three systems (**FTF**, **TFTFT**, and **6T**) (Table 3). Apart from **TFT**, the trend otherwise agrees with the measured FET mobility trends where **FTF** is predicted to have higher mobilities than **TFTFT** and **6T**, which is greater than **TFT**. The magnitudes of the hole versus electron effective masses do not show significant enough differences to estimate theoretically the favoring of n- vs p-type charge transport. According to these calculations, it appears these systems would be ambipolar; however, all of the fluorinated-arene systems appear to favor hole transport, and **6T** is predicted to have favored electron transport. To understand better the directional mobilities within the crystal packing, plots of the planes in real space corresponding to the directions calculated in reciprocal space were made using the program Mercury[75−77] (Figures 9 and 10).

Bandwidths from the HOMO/LUMO tight-binding model dimer splitting cannot be directly compared to the calculated band structures because of the degenerate nature of the conduction bands found in **TFTFT**, **TFT**, and **6T**. It should also be noted in the band structure calculations that the bandwidths of the valence and conduction bands are from multiple split bands. However, the bandwidths can be estimated by evaluating the width of the bands from the total density of states (TDOS); these are summarized in Table 4. **FTF** does not show band degeneracy.

An analysis of the partial densities of states (PDOS) allows us to clarify the origin of the charge densities contributing to the frontier bands. We found that the majority of the charge density contributions arise from the p-orbitals which make up the π-conjugation, in agreement with the above molecular orbital analysis. In general, the three systems show contributions mainly from the conjugated carbon backbone for both the valence and conduction bands. The sulfur p-orbitals contribute mainly to the conduction band, and the electron-withdrawing fluorocarbon fragments appear to make little contribution to the valence/conduction energy level interactions, in agreement with the molecular orbital analysis above. As expected, the calculated band gap values are significantly underestimated. A comparison of the band gap values for three modified structures and the **6T** structure shows a good agreement with experimental trends,[17] where **6T** has the smallest band gap (1.38 eV) followed in order by **FTF** (1.44 eV), **TFTFT** (1.72 eV), and **TFT** (1.97 eV), see Table 1. **FTF**, **TFTFT**, and **6T** have an indirect band gap, whereas **TFT** has a direct band gap.

IV. Discussion

For the perfluoroarene-oligothiophene molecules investigated, orbital contour plots indicate that the greatest charge-density contributions to the valence bands are from the conjugated carbon backbone of the molecular π-system, while the sulfur atoms contribute principally to the conduction band, in agreement with previous work on thiophene oligomers.[61] Very little direct charge-density contribution to the HOMOs and LUMOs is derived from the fluorocarbon groups, although the fluorinated components inductively stabilize the electronic levels of the molecular systems. The analyses from the density of states calculated from the band structures indicate similar trends in charge density distribution within the molecular structures as was seen in the dimer studies. Previous work showed that the S···S, as well as C···C and C···S, intermolecular interactions are key contributors to dispersion in the bands. In particular, it has been suggested that the sulfur−sulfur overlap leads to the dispersion seen in the band structures and dominates the transport properties.[78] In the present study, the band structure

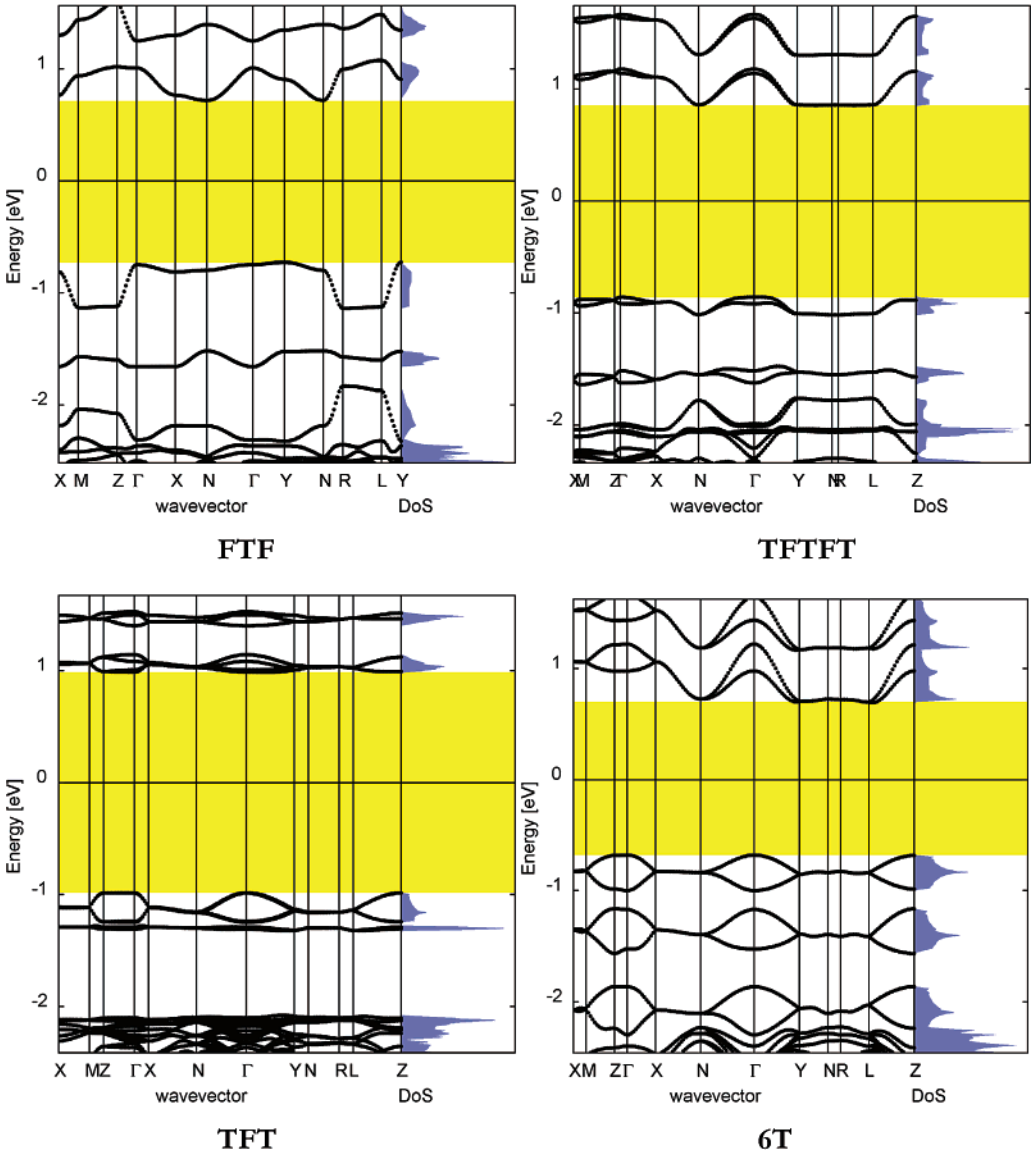

Figure 8. Band structure and density of states (DoS) plots for the semiconductors investigated. The yellow region corresponds to the band gap.

TABLE 3: Comparison of Calculated Effective Masses in the Directions Indicated for the Semiconductors Examined Here

	valence band	conduction band
FTF	$0.29m_e$ (Y−L)	$0.41m_e$ (N−R)
TFTFT	$0.88m_e$ (Γ-Z)	$1.32m_e$ (L$^{\alpha}$-Z)
TFT	$0.38m_e$ (Γ-X)	$0.52m_e$ (Γ-X)
6T	$2.74m_e$ (Z−M)	$1.20m_e$ (L$^{\alpha}$-Z)

calculations agree with previous work revealing substantial sulfur−sulfur interactions, also seen in the present molecular orbital contour plots for the LUMOs. Additional investigation is needed to probe the exact nature of the S···S effects on the transport properties, in particular when vibronic coupling is important.

The applicability of the quantum chemical tight-binding type approach is based on the assumption that in the absence of other effects such as polaron formation,[79−82] one may assume, all other things being equal, that the greater the bandwidth, the greater the carrier mobility (effectively, because scattering out of the band is minimized). The general trend (see Table 2) observed here is that **FTF** has a greater bandwidth than **TFTFT** and **TFT**, in agreement with experimental data showing that **FTF** has a greater carrier mobility than **TFTFT**, followed by **TFT**. In the

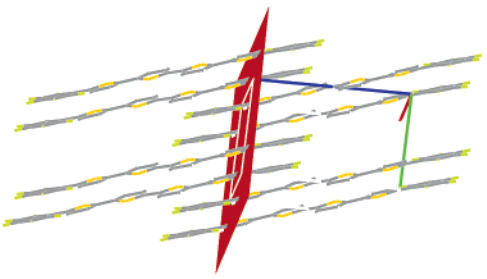

Figure 9. **FTF** crystal packing showing planes of high transport probability. The red plane indicates the direction of favored n-type and p-type transport (001), although the displacements in reciprocal space differ. The *abc* vectors for the crystallographic repeat unit are indicated by the red (*a*), green (*b*), and blue (*c*) lines.

true dimer model, **TFT** appears to have larger bandwidths over **TFTFT**; this is because of the crystallographic packing where the best orbital overlap for **TFTFT** is along the slippage plane (see Figure 10). The computed **6T** bandwidths indicate smaller mobilites than **FTF** but approximately the same as **TFTFT**, in agreement with experiment.[17] However, the transition to n-type conduction in **FTF** is not suggested by the present calculations. In the true and modified dimer models from the crystal cell, smaller bandwidths are observed, indicating reduced molecular

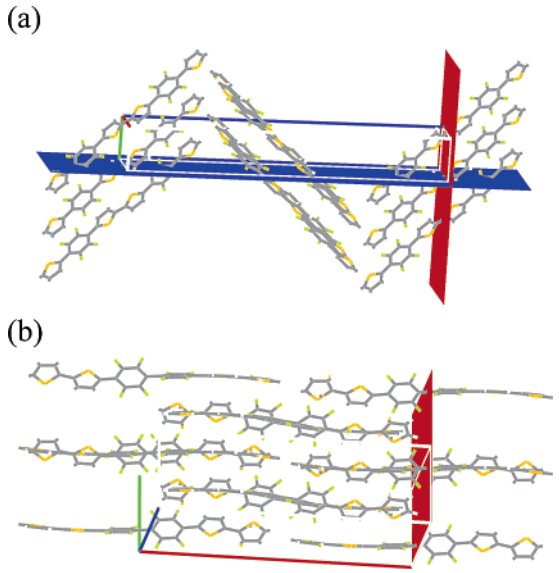

Figure 10. (a) **TFTFT** crystal packing showing planes of highest transport; the blue and red plane indicates the favored n- and p-type transport (010) and (00$\bar{1}$), respectively. (b) **TFT** crystal packing showing the plane of highest transport; the red plane indicates the favored n- and p-type transport direction ($\bar{1}$00). The *abc* vectors for the crystallographic repeat unit are indicated by the red (*a*), green (*b*), and blue (*c*) lines.

TABLE 4: Bandwidths Computed from the Total Densities of States

	valence band (eV)	conduction band (eV)
FTF	0.43	0.313
TFTFT	0.188	0.25
TFT	0.26	0.175
6T	0.45	0.65

interactions. The orbital overlap in $(\mathbf{FTF})_2$ and $(\mathbf{TFT})_2$ is greater in the modified dimer model than in the true dimer which shows staggering (Table 2). Although the general trends of HOMO versus LUMO bandwidths in the modified dimer model may not concur with observed charge polarity, the modified dimer model may give a better indication of the real crystal interactions since, in the crystal structure, staggering is seen where half molecules are interacting with other half molecules for the **FTF** and **TFT** molecular systems. When the true dimer model is compared to the modified dimer model, the bandwidths of **FTF** are seen to increase significantly in the latter, indicating good orbital overlap, whereas in **TFT**, there is less increase because of orbital overlap disruption from the twist in molecular geometry. In the dimer models from the crystal cell, the HOMO splitting is again seen to be greater than that of the LUMO for $(\mathbf{FTF})_2$ and $(\mathbf{TFT})_2$, but not for $(\mathbf{TFTFT})_2$, in variance with the perfect dimer model, but it does correspond to the wider LUMO band seen in the calculated total DOS (Table 4). In the perfect dimer model, greater HOMO than LUMO orbital splittings are observed (Table 2). The greater bandwidths calculated in the perfect dimer model arise from the assumed idealized $\pi-\pi$ stacking. Energy gaps, E_{gap}, for the three models are ordered as follows: modified dimer > true dimer > perfect dimer.

Both steric and electronic interactions are important in the determination of molecular interactions in the $\pi-\pi$ stacking direction. In **FTF** and **TFTFT**, the molecules are nearly planar. So these molecular systems stack well in the *z* direction and have strong $\pi-\pi$ stacking interactions, as indicated in the calculations (e.g., Table 2). However, in **TFT**, because of the significant torsional angle between the two central perfluoroarene rings, the $\pi-\pi$ stacking interactions are much weaker. This disruption in molecular interaction correlates well with the lower observed charge carrier mobilities of this system. This trend is evident in the molecular orbital picture (the bandwidths are substantially smaller than in the other two systems). In the band structure results, the predicted mobility, based on effective mass, agrees with the **FTF** and **TFTFT** trends but does not seem to consider the geometric twist in **TFT** and will be further investigated below.

The band structure calculations agree with experimental trends in band gaps (E_g), where E_g follows **FTF** < **TFTFT** < **TFT**. However, because of the well-known overbinding effects of the DFT functional used,[83] band-gap magnitudes are underestimated by ~0.5−0.8 eV. While DFT-derived trends should be reliable, molecular band gaps calculated using a hybrid functional are, as expected, in much better agreement with the experimentally measured gaps (see Table 1).

Previous electronic structure calculations for **6T** focused on dispersion relations evaluated in four different reciprocal space directions.[78] In this study, we evaluate the structure by including additional directions in reciprocal space to attain a better understanding of the extended electronic structure for comparison to the dimer calculations. In the present reciprocal space evaluation, band dispersions are observed that agree with previously published work by Haddon,*et. al.*[78] Evaluating the CBE and VBE in our **6T** investigation of the standard Brillouin zones, we find the forward directions of the CBE(00$\bar{1}$) and the VBE (101) to have very flat bands, while the unconventional reciprocal space directions show the greatest dispersion in the ($\bar{1}$00) direction for the valence band and in the (010) direction for the conduction band.

The band structures calculated for the standard Brillouin zone directions and the sampling of reciprocal space both reveal band degeneracy predominately in the conduction bands of **TFTFT**, **TFT**, and **6T** (energy degeneracy for particular points in k-space): all three systems have p-type charge carrier mobilities found experimentally through FET measurements. Band degeneracy may occur because of the symmetry of the molecular system leading to degenerate energy levels.[84,85] No band degeneracy is seen in **FTF**, a system with one molecule in the crystal unit cell. In systems with more than one molecule in the crystal unit cell, band degeneracy, which can facilitate phonon scattering[86] and hence reduce carrier mobility, is commonly observed.

The lowest-effective mass is found for **FTF**, which correlates with the highest experimental charge carrier mobility determined in this series. However, for the perfluorinated-oligothiophene systems, all effective masses estimate holes lower than those calculated for electron transport, suggesting that all three systems studied should favor p-type carrier mobilities. For **6T**, it appears that electron transport may be favored; however, the LUMO/conduction band levels are much higher in energy than in the perfluorinated systems. Effective masses for holes and electrons for all systems are on very similar numeric scales, although these systems may appear to slightly favor hole transport, they may also have similar transport probabilities for electrons, indicating these systems should all be ambipolar.

Although the bandwidths may not be directly compared because of the band degeneracy seen in **TFTFT**, **TFT**, and **6T**, both **6T** and **TFTFT** show larger bandwidths for the conduction band, indicating the capacity for n-type charge transport. We believe the rather large conduction bandwidths of **TFTFT** and

6T, although contributed by degenerate bands, indicate potential n-type behavior under optimum processing/fabrication conditions.

The large widths of the **6T** conduction band are in agreement with electronic structure calculations for polythiophene indicating that the conduction bandwidth is greater than the valence bandwidth.[61] The conditions under which the organic FETs are fabricated (and mobility and charge carrier signs are measured) may introduce interfacial artifacts and other effects that are not accounted for in the present calculations.[87−92] Chua et al. recently reported an organic semiconductor electron affinity in agreement with our earlier work[14,15] and showed, not unexpectedly, that removing hydroxyl trapping sites at the semiconductor−dielectric interface can be important for mobilizing n-type FET charge carriers.[93,94] The present calculations indicate, generally, that oligothiophene-fluoroarenes should exhibit ambipolar transport[43] (based on idealized behavior with perfect molecular crystals). The experimental electron affinities obtained from the film electrochemistry suggest little difference between **FTF** and **TFTFT**, also shown in our theoretical models. The effective masses also suggest that all these materials may be ambipolar, with the carrier sign determined by the experimental fabrication conditions and measurement schemes.

To better understand the origin of the mobility in certain crystallographic directions, planes were plotted in real space corresponding to the directions calculated in reciprocal space (Figures 9 and 10). In plotting the planes that correspond to the directions of highest-predicted mobility for the three systems, we found that the greatest mobility is in the $\pi-\pi$ stacking direction. For **FTF**, the largest mobility predicted for both n- and p-type carriers is in the $\pi-\pi$ stacking direction, the $(00\bar{1})$-vector direction at different displacements in reciprocal space. Figure 9 shows a plot of the planes for **FTF**. For **TFTFT**, the highest-symmetry plane for both the n- and p-type regime shows favorable transport in the $\pi-\pi$ stacking direction, (010) and $(00\bar{1})$, respectively. On the basis of the crystal packing motifs, **FTF** has one defined orientation in which the long axis of the molecule may align flat with the substrate, whereas in **TFTFT**, there are several directions of orientation for this alignment. The twist in **TFT** renders it difficult to discern what planes intersect, but it appears that the $\pi-\pi$ stacking interactions are also important, although they are substantially disrupted by the molecular twist, leading to lower carrier mobilities. Figure 10 shows the planes of high transport probability for **TFTFT** and **TFT**.

V. Conclusions

In summary, we find that analyses of computed orbital splitting trends and band structure can elucidate charge-transport behavior in these unusual isomeric molecular crystals. We find narrow bands and comparable effective masses in both conduction and valence bands in all systems studied. This suggests that transport is intrinsically ambipolar, with other issues (trapping, injection, phonon coupling, and measurement technique) possibly dominating the result of any given sample set or measurement method. Steric effects in **TFT** compromise molecular planarity and render it a far poorer conductor than planar **TFTFT** or **FTF**. This indicates (in agreement with a simple tight-binding picture) that the extent of $\pi-\pi$ overlap determines the dominant transport direction.

Acknowledgment. The authors thank Drs. F. Arnold, G. Hutchison, A. Troisi, C. Risko, K. Shuford, O. Kontsevoi, and other members of the Ratner group for helpful discussions. We thank Dr. S. Ohlinger from Wave function Inc. for assistance in troubleshooting the orbital plot calculations. We thank the NSF/MRSEC program through the Northwestern MRSEC (DMR-0076097), as well as the ONR (N00014-02-1-0909) for support of this research.

References and Notes

(1) Facchetti, A.; Yoon, M.-H.; Marks, T. J. *Adv. Mater.* **2005**, *17*, 1705.
(2) Brédas, J.-L.; Deljonne, D.; Coropceanu, V.; Cornil, J. *Chem. Rev.* **2004**, *104*, 4971.
(3) Bendikov, M.; Wudl, F.; Perepichka, D. F. *Chem. Rev.* **2004**, *104*, 4891.
(4) Hannewald, K.; Bobbert, P. A. *Appl. Phys. Lett.* **2004**, *85*, 1535.
(5) Sirringhaus, H.; Brown, P. J.; Friend, R. H.; Nielsen, M. M.; Bechgaard, K.; Langeveld-Voss, B. M. W.; Spiering, A. J. H.; Janssen, R. A. J.; Meijer, E. W.; Herwig, P.; de Leeuw, D. M. *Nature (London)* **1999**, *401*, 685.
(6) Janzen, D. E.; Burand, M. W.; Ewbank, P. C.; Pappenfus, T. M.; Higuchi, H.; da Silva Filho, D. A.; Young, V. G.; Brédas, J.-L.; Mann, K. R. *J. Am. Chem. Soc.* **2004**, *126*, 15295.
(7) Fichou, D. *J. Mater. Chem.* **2000**, *10*, 571.
(8) Horowitz, G.; Hajlaoui, M. E. *Adv. Mater.* **2000**, *12*, 1046.
(9) Maud, J. M. *Synth. Met.* **1999**, *101*, 375.
(10) Mushrush, M.; Facchetti, A.; Lefenfeld, M.; Katz, H. E.; Marks, T. J. *J. Am. Chem. Soc.* **2003**, *125*, 9414.
(11) Schoonbeek, F. S.; Van Esch, J. H.; Wegewijs, B.; Rep, D. B. A.; De Haas, M. P.; Klapwijk, T. M.; Kellogg, R. M.; Feringa, B. L. *Angew. Chem., Int. Ed.* **1999**, *38*, 1393.
(12) Lovinger, Andrew J.; Davis, D. D.; Dodabalapur, A.; Katz, H. E. *Chem. Mater.* **1996**, *8*, 2836.
(13) Katz, H. E.; Torsi, L.; Dodabalapur, A. *Chem. Mater.* **1995**, *7*, 2235.
(14) Facchetti, A.; Mushrush, M.; Yoon, M.-H.; Hutchison, G. R.; Ratner, M. A.; Marks, T. J. *J. Am. Chem. Soc.* **2004**, *126*, 13859.
(15) Facchetti, A.; Yoon, M.-H.; Stern, C. L.; Hutchison, G. R.; Ratner, M. A.; Marks, T. J. *J. Am. Chem. Soc.* **2004**, *126*, 13480.
(16) Demanze, F.; Cornil, J.; Garnier, F.; Horowitz, G.; Valat, P.; Yassar, A.; Lazzaroni, R.; Brédas, J.-L. *J. Phys. Chem. B* **1997**, *101*, 4553.
(17) Facchetti, A.; Yoon, M.-H.; Stern, C. L.; Katz, H. E.; Marks, T. J. *Angew. Chem., Int. Ed.* **2003**, *42*, 3900.
(18) Facchetti, A.; Mushrush, M.; Katz, H. E.; Marks, T. J. *Adv. Mater.* **2003**, *15*, 33.
(19) Chesterfield, R. J.; Newman, C. R.; Pappenfus, T. M.; Ewbank, P. C.; Haukaas, M. H.; Mann, K. R.; Miller, L. L.; Frisbie, C. D *Adv. Mater.* **2003**, *15*, 1278.
(20) Pappenfus, T. M.; Chesterfield, R. J.; Frisbie, C. D.; Mann, K. R.; Casado, J.; Raff, J. D.; Miller, L. L. *J. Am. Chem. Soc.* **2002**, *124*, 4184.
(21) Newman, C. R.; Frisbie, C. D.; da Silva Filho, D. A.; Brédas, J.-L.; Ewbank, P. C.; Mann, K. R. *Chem. Mater.* **2004**, *16*, 4436.
(22) Hapiot, P.; Demanze, F.; Yassar, A. Garnier, F. *J. Phys. Chem.* **1996**, *100*, 8397.
(23) Raya, A.; Mora, M. A. *Polymer* **2004**, *45*, 6391.
(24) Cornil, J.; Gueli, I.; Dkhissi, A.; Sancho-Garcia, J. C.; Hennebicq, E.; Calbert, J. P.; Lemaur, V.; Beljonne, D.; Brédas, J.-L. *J. Chem. Phys.* **2003**, *118*, 6615.
(25) Kunugi, Y.; Takimiya, K.; Yamane, K.; Yamashita, K.; Aso, Y.; Otsubo, T. *Chem. Mater.* **2003**, *15*, 6.
(26) Ponomarenko, S. A.; Kirchmeyer, S.; Elschner, A.; Huisman, B.-H.; Karbach, A.; Drechsler, D. *Adv. Funct. Mater.* **2003**, *13*, 591.
(27) Afzali, A.; Dimitrakopoulos, C. D.; Breen, T. *J. Am. Chem. Soc.* **2002**, *124*, 8812.
(28) Mitzi, D. B.; Dimitrakopoulos, C. D.; Kosbar, L. L. *Chem. Mater.* **2001**, *13*, 3728.
(29) Dimitrakopoulos, C. D. Malenfant, P. R. L. *Adv. Mater.* **2002**, *14*, 99.
(30) Wurthner, F. *Angew. Chem., Int. Ed.* **2001**, *40*, 1037.
(31) Dimitrakopoulos, C. D.; Mascaro, D. J. *IBM J. Res. Dev.* **2001**, *45*, 11.
(32) Kraft, A *ChemPhysChem* **2001**, *2*, 163.
(33) Meng, H.; Bendikov, M.; Mitchell, G.; Holgeson, R.; Wudl, F.; Bao, Z.; Siegrist, T.; Kloc, C.; Chen, C.-H. *Adv. Mater.* **2003**, *15*, 1090.
(34) Videlot, C.; Ackermann, J.; Blanchard, P.; Raimundo, J.-M.; Frere, P.; Allain, M.; de Bettignies, R.; Levillain, E.; Roncali, J. *Adv. Mater.* **2003**, *15*, 306.
(35) Halik, M.; Klauk, H.; Zschieschang, U.; Scmid, G.; Ponomarenko, S.; Kiechmayer, S.; Weber, W. *Adv. Mater.* **2003**, *15*, 917.
(36) Ito, K.; Suzuki, T.; Sakamoto, Y.; Kubota, D.; Inoue, Y.; Sato, F.; Tokito, S. *Angew. Chem., Int. Ed.* **2003**, *42*, 1159.
(37) Sandberg, H.; Henze, O.; Kilbinger, A. F. M.; Sirringhaus, H.; Feast, W. J.; Friend, R. H. *Synth. Met.* **2003**, *137*, 885.

(38) Meng, H.; Zheng, J.; Lovinger, A. J.; Wang, B.-C.; Van Patten, P. G.; Bao, Z. *Chem. Mater.* **2003**, *15*, 1778.
(39) Kunugi, Y.; Takimiya, K.; Yamashita, K.; Aso, Y.; Otsubo, T. *Chem. Lett.* **2002**, *31*, 958.
(40) Sakamoto, Y.; Suzuki, T.; Kobayashi, M.; Gao, Y.; Fukai, Y.; Inoue, Y.; Sato, F.; Tokito, S. *J. Am. Chem. Soc.* **2004**, *126*, 8138.
(41) Yoon, M.-H.; Facchetti, A.; Stern, C. E.; Marks, T. J. *J. Am. Chem. Soc.* **2006**, *128*, 5792−5801.
(42) Facchetti, A.; Letizia, J.; Yoon, M.-H.; Mushrush, M.; Katz, H. E.; Marks, T. J. *Chem. Mater.* **2004**, *16*, 4715.
(43) Yoon, M.-H.; DiBenedetto, S. A.; Facchetti, A.; Marks, T. J. *J. Am. Chem. Soc.* **2005**, *127*, 1348.
(44) Jones, B. A.; Ahrens, M. J.; Yoon, M.-H.; Facchetti, A.; Marks, T. J. *Angew. Chem., Int. Ed.* **2004**, *43*, 6363.
(45) Facchetti, A.; Deng, Y.; Wang, A.; Koide, Y.; Sirringhaus, H.; Marks, T. J.; Friend, R. H. *Angew. Chem., Int. Ed.* **2000**, *39*, 4547.
(46) Garnier, F.; Yassar, A.; Hajlaoui, R.; Horowitz, G.; Deloffre, F.; Servet, B.; Ries, S.; Alnot, P. *J. Am. Chem. Soc.* **1993**, *115*, 8716.
(47) Brocks, G. *J. Chem. Phys.* **2000**, *112*, 5353.
(48) Brocks, G. *Synth. Met.* **2001**, *119*, 253.
(49) Endes, R. G.; Fong, C. Y.; Yang, L. H.; Witte, G.; Wöll, Ch. *Comput. Mater. Sci.*. **2004**, *29*, 362.
(50) Siegrist, T.; Kloc, C.; Laudise, R. A.; Katz, H. E.; Haddon, R. C. *Adv. Mater.* **1998**, *10*, 379.
(51) Troisi, A.; Orlandi, G. *J. Phys. Chem. B* **2005**, *109*, 1849. [Note: For pentacene, band structures are a good starting point and the vibronic variation of the tunneling matrix element (or bandwidths) determines resistivity comparatively, see Troisi, A.; Orlandi, G. *Phys. Rev. Lett.* **2006**, *96*, 086601.]
(52) Fabiano, E.; Della Sala, F.; Cingoland, R.; Weimer, M.; Görling, A. *J. Phys. Chem.* **2005**, *109*, 3078.
(53) Tsai, F.-C.; Chang, C.-C.; Liu, C.-L.; Chen, W.-C.; Jenekhe, S. A. *Macromolecules* **2005**, *38*, 1958.
(54) Cao, H.; Ma, J.; Zhang, G.; Jiang, Y. *Macromolecules* **2005**, *38*, 1123.
(55) Hutchison, G. R.; Ratner, M. A.; Marks, T. J. *J. Phys. Chem. B* **2005**, *109*, 3126.
(56) Hutchison, G. R.; Ratner, M. A.; Marks, T. J. *J. Am. Chem. Soc.* **2005**, *127*, 2339.
(57) Salzner, U.; Lagowski, J. B.; Pickup, P. G.; Poirier, R. A. *Synth. Met.* **1998**, *96*, 177.
(58) Salzner, U. *Synth. Met.* **2001**, *119*, 215.
(59) Delley, B. *J. Chem. Phys.* **2000**, *113*, 7756 and references therein.
(60) Ye, L.; Freeman, A. J.; Ellis, D. E.; Delley, B. *Phys. Rev. B* **1989**, *40*, 6277.
(61) Hutchison, G. R.; Zhao, Y.-J.; Delley, B.; Freeman, A. F.; Ratner, M. A.; Marks, T. J. *Phys. Rev. B* **2003**, *68*, 035204.
(62) Kong, J.; White, C. A.; Krylov, A. I.; Sherrill, C. D.; Adamson, R. D.; Furlani, T. R.; Lee, M. S.; Lee, A. M.; Gwaltney, S. R.; Adams, T. R.; Ochsenfeld, C.; Gilbert, A. T. B.; Kedziora, G. S.; Rassolov, V. A.; Maurice, D. R.; Nair, N.; Shao, Y.; Besley, N. A.; Maslen, P. E.; Dombroski, J. P.; Dachsel, H.; Zhang, W. M.; Korambath, P. P.; Baker, J.; Byrd, E. F. C.; Van Voorhis, T.; Oumi, M.; Hirata, S.; Hsu, C. P.; Ishikawa, N.; Florian, J.; Warshel, A.; Johnson, B. G.; Gill, P. M. W.; Head-Gordon, M.; Pople, J. A. *J. Comput. Chem.* **2000**, *21*, 1532.
(63) Becke, A. D. *J. Chem. Phys.* **1993**, *98*, 5648.
(64) Lee, C.; Yang, W.; Parr, R. G. *Phys. Rev. B* **1988**, *37*, 785.
(65) *Jaguar 5.0*; Schrödinger, LLC.: Portland, OR, 2002.
(66) *Spartan 04*; Wavefunction, Inc.: Irvine, CA, 2001.
(67) Delley, B. *J. Chem. Phys.* **1990**, *92*, 508.
(68) Perdew, J. P.; Wang, Y. *Phys. Rev. B* **1992**, *45*, 13244.
(69) Shapley, W. A.; Chong, D. P. *Int. J. Quantum Chem.* **2001**, *81*, 34.
(70) Siegrist, T.; Fleming, R. M.; Haddon, R. C.; Laudise, R. A.; Lovinger, A. J.; Katz, H. E.; Bridenbaugh, P.; Davis, D. D. *J. Mater. Res.* **1995**, *10*, 2170.
(71) Allen, F. H. *Acta Crystallogr.* **2002**, *B58*, 380.
(72) Blochl, P. E.; Jepsen, O.; Andersen, O. K. *Phys. Rev. B* **1994**, *49*, 16223.
(73) Pope, M.; Swenberg, C. E. *Electronic Processes in Organic Crystals and Polymers*, 2nd ed.; Oxford University Press: New York, 1999; p. 43.
(74) Huang, J.; Kertesz, M. *J. Chem. Phys.* **2005**, *122*, 234707.
(75) Bruno, I. J.; Cole, J. C.; Edgington, P. R.; Kessler, M. K.; Macrae, C. F.; McCabe, P.; Pearson, J.; Taylor, R. *Acta Crystallogr.* **2002**, *B58*, 389.
(76) Taylor, R.; Macrae, C. F. *Acta Crystallogr.* **2001**, *B57*, 815.
(77) *Mercury 1.3*; The Cambridge Crystallographic Data Centre: Cambridge, U.K., 2001.
(78) Haddon, R. C.; Siegrist, T.; Fleming, R. M.; Bridenbaugh, P. M.; Laudise, R. A. *J. Mater. Chem.* **1995**, *5*, 1719.
(79) Cheng, Y. C.; Silbey, R. J.; da Silva Filho, D. A.; Calbert, J. P.; Cornil, J.; Brédas, J.-L. *J. Chem. Phys.* **2003**, *118*, 3764.
(80) Sancho-García, J. C.; Brédas, J.-L. Beljonne, D.; Cornil, J.; Martínez- Álvarez, R.; Hanack, M.; Poulsen, L.; Gierschner, J.; Mack, H.-G.; Egelhaaf, H.-J.; Oelkrug, D. *J. Phys. Chem. B* **2005**, *109*, 4872.
(81) da Silva Filho, D. A.; Kim, E.-G.; Brédas, J.-L. *Adv. Mater.* **2005**, *17*, 1072.
(82) Dkhissi, A.; Beljonne, D.; Lazzaroni, R.; Louwet, F.; Groenendaal, L.; Brédas, J.-L. *Int. J. Quant. Chem.* **2003**, *91*, 517.
(83) Koch, W.; Holthausen, M. C. *A Chemist's Guide to Density Functional Theory*, 2nd ed; Wiley-VCH: Weinheim, Germany, 2000.
(84) Clerc, F.; Bovet, M.; Berger, H.; Despont, L.; Koitzsch, C.; Gallus, O.; Patthey, L.; Shi, M.; Krempasky, J.; Garnier, M. G.; Aebi, P. *J. Phys.: Condens. Matter* **2004**, *16*, 3271.
(85) Dunaevskii, S. M. *Phys. of Solid State* **2001**, *43*, 2257.
(86) Miyatsuji, K.; Masaki, K.; Ravaioli, U. *J. Appl. Phys.* **1996**, *79*, 911.
(87) Knupfer, M.; Peisert, H. *Phys. Status Solidi* **2004**, *201*, 1055.
(88) Gao, W.; Kahn, A. *J. Phys.: Condensed Matter* **2003**, *15*, S2757.
(89) Gao, W.; Kahn, A. *Appl. Phys. Lett.* **2003**, *82*, 4815.
(90) Garnier, F. *Chem. Phys.* **1998**, *227*, 253.
(91) Riess, W.; Riel, H.; Beierlein, T.; Brütting, W.; Müller, P.; Seidler, P. F. *J. Res. Dev.* **2001**, *45*, 77.
(92) Rep, D. B. A.; Morpurgo, A. F.; Sloof, T. M.; Klapwijk, T. M. *J. Appl. Phys.* **2003**, *93*, 2082.
(93) Chua, L.-L.; Zaumseil, J.; Chang, J.-F.; Ou, E. C.-W.; Ho, P. K.-H.; Sirringhaus, H.; Friend, R. H. *Nature (London)* **2005**, *434*, 194.
(94) Yoon, M.-H.; Kim, C.; Facchetti, A.; Marks, T. J. *J. Am. Chem. Soc.* **2006**, *128*, 12851.